www.amlett.com, www.vbripress.com/aml, DOI: 10.5185/amlett.2014.7591 Published online by the VBRI press in 2014

Growth characteristics of glancing angle deposited (GLAD) thin films

Alireza Dolatshahi-Pirouz[1,2*]

[1]*Interdisciplinary Nanoscience Center (iNANO), Aarhus University, DK-8000 Aarhus C, Denmark*
[2]*Department of Physics and Astronomy, Aarhus University, DK-8000 Aarhus C, Denmark*

[*]Corresponding author. Tel: (+45) 22879762; E-mail: aldo@inano.au.dk

Received: 07 July 2014, Revised: 27 July 2014 and Accepted: 03 August 2014

ABSTRACT

This paper investigates the effect of surface diffusion and re-emission on the surface morphology of GLAD thin films. This was done through GLAD of platinum and tantalum at two different surface temperatures (293 K and 153 K). The effect of shadowing during the thin film growth was examined by utilizing Atomic force microscopy (AFM) to determine the root-mean square (rms) value, the surface roughness, and thus the growth exponent β. Our results showed that β was not affected by substrate temperature during deposition, however it increased from $\beta = 0.47 \pm 0.06$ to $\beta = 0.94 \pm 0.12$ as the thin film material was switched from platinum to tantalum. The change in the growth exponent β indicates that the kinetics of the film growth at grazing incidence are primarily influenced by re-emission and shadowing effects with surface diffusion playing a minor role.

Keywords: GLAD; shadowing effect; nanotopography; surface diffusion; thin film scaling behavior.

Alireza Dolatshahi-Pirouz received his PhD in physics from Aarhus University. In 2011 he was awarded the prestigious Sapere Aude Eliteforsker award and moved to Boston to conduct his postdoctoral research at the Wyss Institute of Biologically Inspired Engineering and MIT. To date he has published 24 papers, which have been cited over 400 times and currently he holds an h-index at 13.

Introduction

Thin film surface morphology is known to influence the performance of materials in areas such as biomaterial science **[1-11]**, catalysis **[12]**, optics **[13-15]**, protein adsorption **[16-18]**. Therefore, there has been a high interest in exploring the dynamics of thin film morphology and surface roughness **[19, 20]**. From a fundamental point of view these studies are of great interest for scientist in the thin film community **[21]**. From an applied point of view it is possible to use this knowledge to control the surface roughness evolution and consequently obtain a better control of important material properties **[3, 21]**. The surface morphology evolution during thin film growth is a complex process which relies on the random noise in the deposition process, non-local shadowing and re-emission effect **[21-25]** and local smoothing effects such as surface diffusion **[21]**. Surface diffusion relies on the surface temperature (T_s) and increases as function of T_s **[26, 27]**. By examining the homologous deposition temperature $\theta = T_s/T_m$ where T_m is the material melting point (T_m) it is possible to unravel the effect of surface diffusion during thin film growth **[26]**. The shadowing effect on the other hand arise, when taller surface features shadow smaller features from receiving the incoming flux leading to a competitive growth, while re-emission is caused by high-energy particles hitting the sidewalls of mound structures and thereby resulting in re-emission of previously adsorped particles. Like surface diffusion re-emission also tends to smoothen the surface, since re-emitted particles can fill out the valleys between mound structures **[22, 23]**.

Typically the morphological evolution of surfaces is described within the context of a dynamic scaling approach **[28-31]**. Here the surface roughness w varies with the surface thickness h as $w \sim h^{\beta}$, in which β is called the growth exponent. The growth exponent β classifies which physical phenomenon dominates the thin film growth process and determines how intense the roughness evolution is **[21]**. For instance $\beta = 1$ is equivalent with a growth process dominated by shadowing effects **[22, 23]**, $\beta = 0.5$ with a random deposition model **[21]** and $\beta \leq 0.25$ is linked to growth processes dominated by surface diffusion **[21]**. Here we use Glancing Angle deposition with rotation to grow nano-rough surfaces with different morphological properties. During GLAD the incoming particles flux impinges on the substrate at an oblique angle **[32, 33]** resulting in an enhanced shadowing effect creating columnar structures, which in turn triggers an intensified re-emission **[22, 23]**. Two different materials were employed in the GLAD experiments. Tantalum, which has

a low homologous temperature at room temperature (θ = 0.09) and platinum with a homologous temperature (θ = 0.14) that is similar to most metals. The thin films are grown at the deposition angles α = 5˚ and 10˚. Moreover the films were fabricated at different deposited surface mass densities in order to determine the dynamical growth exponent β. In case of platinum a lower surface temperature at 153 K was used to obtain as similar homologous temperatures as tantalum at room temperature. The reported results show that the growth exponent β is appreciable lower for the platinum depositions as compared to tantalum at both T_s = 293 K and 153 K, while no apparent differences were observed between the two deposition angles α = 5˚ and 10˚. Overall, our results indicate that surface diffusion does not contribute to the thin film growth process, whereas the shadowing effect dominated the process with minor contribution from secondary re-emission processes. This new knowledge can be used to design improved nanostructured GLAD surfaces, which can be applied to a broad range of materials including, biomaterials, optical materials and biosensors.

Experimental

The platinum thin films (Platinum from Dansk Ædelmetal A/S, DK; purity 99.9 %) were grown on either gold coated silicon or gold coated quartz crystals (q-sense) by e-gun evaporation in a vacuum of about 10^{-8} bar. The evaporation was performed at room temperature without substrate rotation and with a distance between the evaporation source and the substrate of 25 cm. The deposition was carried out at the oblique deposition angles θ of 10˚ and 5˚. The deposition angle θ was determined with a precision of < 1° and defined as 90° when the substrate was perpendicular to the incoming flux. For each deposition angle, the surface mass density (ρ) (representing the total deposited mass per area) was varied from a series of surface mass densities of $2.2 \cdot 10^{-5}$ g/cm^2 , $4.3 \cdot 10^{-5}$ g/cm^2, $8.2 \cdot 10^{-5}$ g/cm^2, $22 \cdot 10^{-5}$ g/cm^2, and $32 \cdot 10^{-5}$ g/cm^2 for the platinum depositions and $6.6 \cdot 10^{-5}$ g/cm^2 , $14.4 \cdot 10^{-5}$ g/cm^2, $20.3 \cdot 10^{-5}$ g/cm^2, $36.05 \cdot 10^{-5}$ g/cm^2 for the tantalum depositions to produce films with different thicknesses, since the surface mass density monitored by the quartz crystal microbalance is proportional to the nominal film thickness (given a constant mass density) **[34]**. The film surface morphology was investigated using atomic force microscopy (AFM), with a commercial Nanoscope IIIa Multimode SPM (Veeco Instruments, Santa Barbara, CA) operated under ambient conditions in the tapping mode at scan frequencies of 1-2 Hz. Conventional Silicon cantilevers (NSG01, NT-MDT, Russia) were used with a typical resonance frequency of 150 kHz, a spring constant of 5.5 N/m, a aspect ratio at 3:1 and a tip radius below 10 nm. To investigate if the conventional cantilever applied in this work would lead to misleading results, test was made with two different types of non-conventional cantilevers. For each film, a series of AFM images of linear dimensions 1 μm, 5.5 μm, and 10 μm was recorded with a resolution of 512×512 pixels at a minimum of three different locations across the surface. The AFM images were subsequently analyzed using a home-written extension to the scanning probe image processor image analysis software package (SPIP) in order to extract the values of the rms roughness, w **[35]**. The rms roughness values displayed in this paper corresponds to the saturated rms-roughness **[35]**. This analysis program divided each image into sub-images, using the size of the subdivision as the length scale L. For each sub-image the rms roughness parameter w was determined, and in this way we could explore the correlation between the rms roughness and length scale L. For a more detailed analysis of the surface morphology plan-view SEM images were acquired by using a Nova NanoSEM 600 (FEI Company).

Results and discussion

In **Fig. 1**(**A-D**) AFM images of the platinum and tantalum films deposited at α =5˚ and 10˚ are shown. Here a clear difference in the surface morphologies is observed for both materials at the different deposition angles. At α = 5˚ the platinum and tantalum surfaces are dominated by sharp columnar surface features. Similar mound structures are observed at α = 10˚, however with less sharp edges.

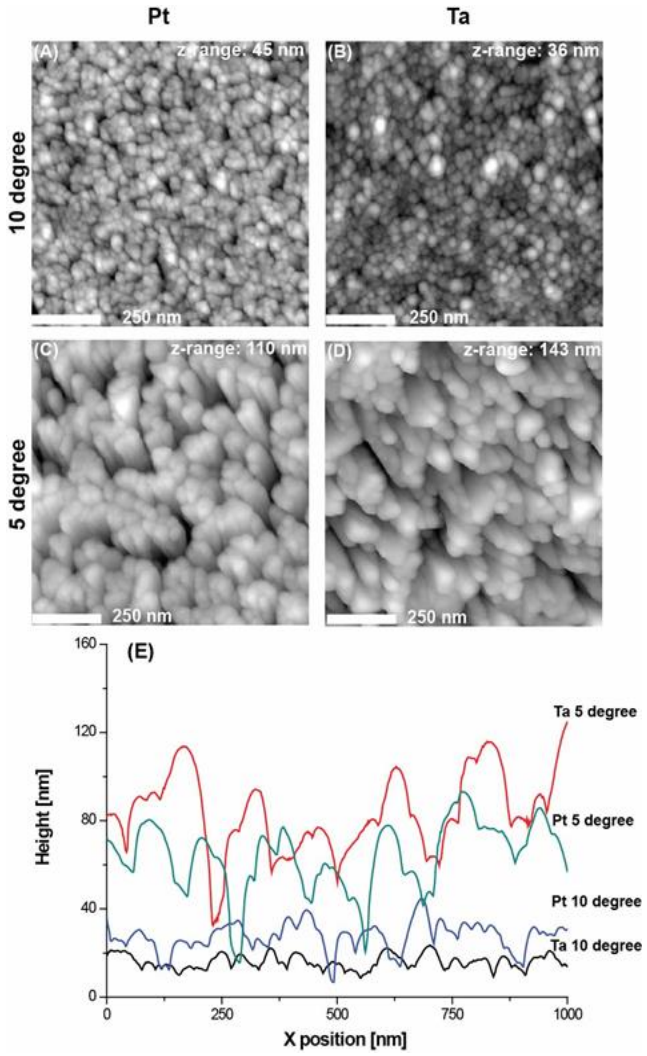

Fig. 1. Representative AFM images of (A)-(B) Tantalum and (C)-(D) platinum. AFM height curves corresponding to the images in figure (A)-(D).

AFM line-scans corresponding to the images in **Fig. 1(A-D)** are shown in **Fig. 1(E)**, from where it is clearly seen that the dispersion in height in general are larger for the depositions carried out at $\alpha = 5^{\circ}$ compared to $\alpha = 10^{\circ}$ in accordance with a more pronounced shadowing effect at lower deposition angles. SEM images were like-wise acquired of the respective surfaces (**Fig. 2(A-D)**). The SEM images revealed small grainy structures on the surfaces deposited at $\alpha = 10^{\circ}$.

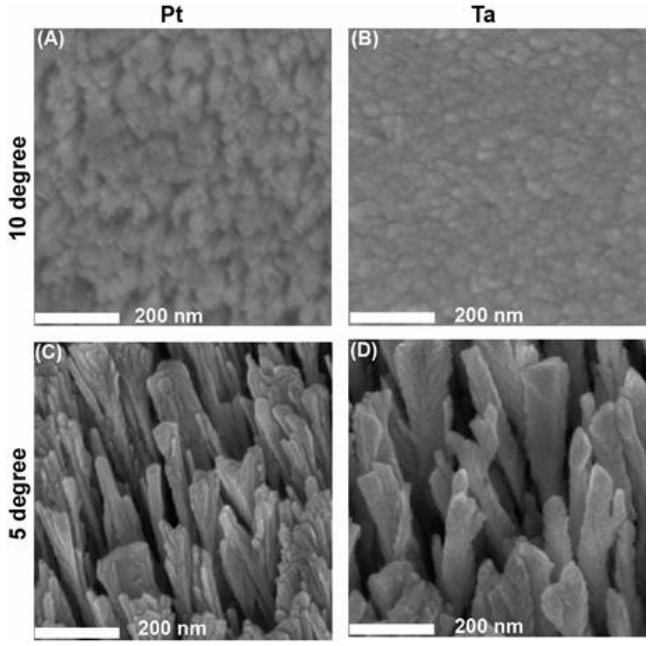

Fig. 2. Representative SEM images of (A)-(B) Platinum and (C)-(D) Tantalum.

On the platinum and tantalum surfaces deposited at $\alpha = 5^{\circ}$ larger and more whisker-like surface protrusions were observed. These surface structures were similar in shape for both materials, however the side-walls of the platinum columns appeared slightly eroded compared to the smoother tantalum columns. Through AFM imaging we were able to retrieve the surface roughness value of the respective surfaces and thus gain a better understanding of the growth mechanism behind the observed surface morphologies. The surface roughness values for platinum and tantalum are displayed in **Fig. 3(A-B)** at $\alpha = 5^{\circ}$ and 10° and different deposited surface mass densities. The roughness values ranged from 3.04 nm to 36.05 nm depending on the specific deposition conditions and the material in question. This clearly demonstrates how GLAD offers unique possibilities to fabricate nano-rough surface morphologies with different properties covering a large roughness span. The data in **Fig. 3(A-B)** were subsequently fitted with a power law, which is in accordance with the relation $w \sim h^{\beta}$, and the growth exponent β was retrieved from the fits shown in **Fig. 3(A-B)**.

These exponents are shown in **Table 1**, from which it is clearly seen that the growth exponents in general are e larger for the tantalum deposition at T_s = 293 K. Interestingly the exponent values where very close to one for the tantalum deposition, while in the case of platinum $\beta \leq 0.5$. Models have shown that β is larger than 0.5, when the shadowing effect dominates the growth process with surface diffusion and re-emission still contributing to the process and close to one when the surface growth is dominated by shadowing effects **[22, 23]**.

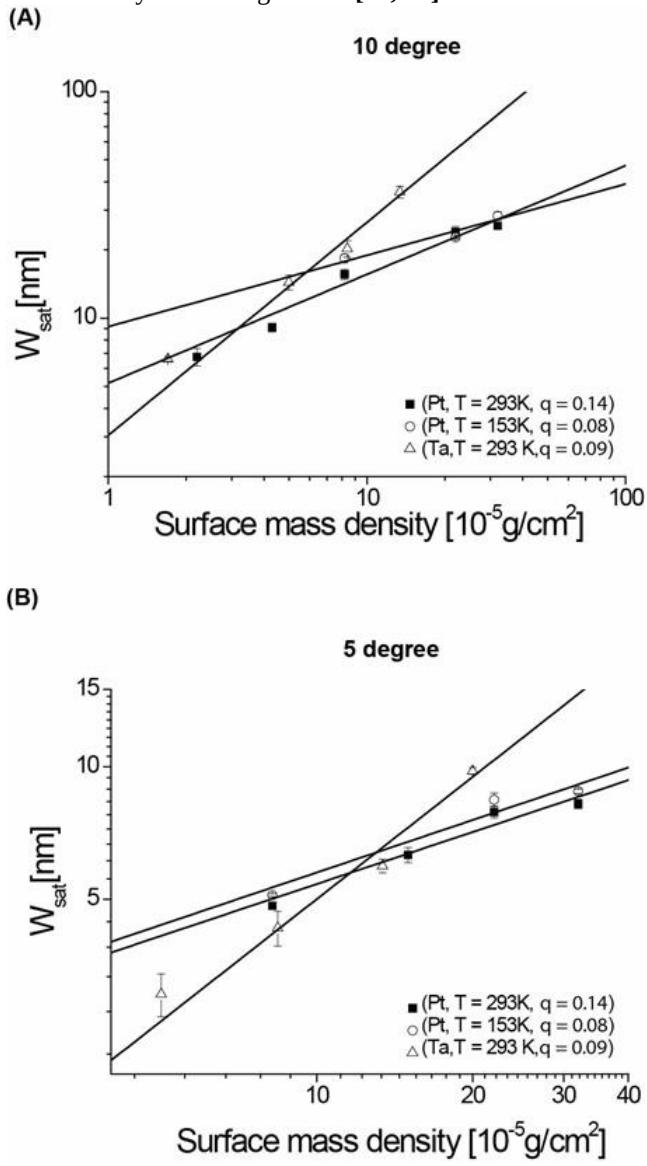

Fig. 3. The relationship between the saturated surface roughness and the amount of mass deposited on the respective surfaces is displayed here for depositions carried out at (A) 10° and (B) 5°. The curves have been fitted with a power law $y = ax^{\beta}$.

From the results in **Table 1** it is therefore plausible to conclude that the tantalum depositions were mainly dominated by shadowing effects with minor contributions from smoothing effects such as re-emission and surface diffusion, whereas smoothing effects (re-emission and diffusion) and geometrical shadowing most like governed the growth front of the platinum surfaces **[1]**[1]. The growth of metallic thin film is typically divided in different growth zones **[26]**. The zone boundaries in this model are

[1]The authors acknowledge that it might be difficult to access the entire surface on the deposition carried out at $\alpha = 5^{\circ}$. However the same growth exponents were acquired for platinum and tantalum for GLAD deposition at $\alpha = 10^{\circ}$, which consisted of a more homogenous and accessible surface structure. Accordingly even if the AFM measurements gives a misinterpretation of the surface morphology at $\alpha = 5^{\circ}$.

determined by the homologous temperature of the experiment in question, for instance $\theta < 0.15$ is defined as zone I, where surface diffusion does not contribute to the surface growth. In the region $0.15 \leq \theta \leq 0.30$ (Zone T) surface diffusion begins to contribute to the growth front and in the regime $\theta \geq 0.30$ (zone II and III) surface diffusion is expected to have a significant impact on the surface morphology[26]. Even though the homologous temperature of platinum was slightly below 0.15 a recent study performed by Mukherjee et al. **[36, 37]** have shown a noticeable influence by surface diffusion in the region $0.11 < \theta < 0.15$. Surface diffusion could therefore be important in the development of the platinum thin film structure, while it is unlikely that surface diffusion contribute to the tantalum thin film growth. To examine this postulation in more detail platinum experiments were carried out at $\theta = 0.08$.

Table 1. Growth exponent values corresponding to the different experimental conditions employed in the GLAD experiments are shown here.

Deposition Condition	10° (Pt, θ = 0.14)	10° (Pt, θ = 0.08)	10° (Pt, θ = 0.09)	5° (Pt, θ = 0.14)	5° (Pt, θ = 0.08)	10° (Pt, θ = 0.09)
β	0.39 ± 0.07	0.396 ± 0.107	0.922 ± 0.117	0.48 ± 0.06	0.32 ± 0.09	0.94 ± 0.12

From **Table 1** it is noted that β did no change significantly and similar β-values for platinum thin film depositions were determined at $T_s = 153$ K and $T_s = 273$ K . The results displayed in **Table 1** therefore indicate that the lower growth exponent values observed for platinum is caused by a more pronounced re-emission effect during the platinum depositions and not surface diffusion. This is a reasonable assumption when taking the material properties of tantalum and platinum into consideration, since tantalum has a higher melting temperature (3290 K) compared to platinum (2041 K), it is much more difficult to detach particles from tantalum as compared to platinum. The SEM images in figure 2(B)-(C) support the results listed in **Table 1**, since the side-walls of the platinum columns showed clear signs of erosion compared to the tantalum structures, which could be a result of a more intensified re-emission process during the platinum depositions. The scenario presented here fits well with the work performed in **[22, 23]**. Here it was shown that surface diffusion did not have any effect on the growth exponent, while a close relationship between re-emission and the growth exponent β was demonstrated. The reason behind this interesting behavior was argued to stem from the local properties of surface diffusion, which were outplayed by the strong non-local shadowing effect.

Conclusion

Platinum and tantalum thin films were grown by GLAD at $\alpha = 5^\circ$ and 10° at the temperatures $T_s = 153$ K and 293 K. The surface morphologies and roughness values were subsequently examined on the respective surface at different deposited surface mass densities by AFM and SEM. From the AFM images the columnar features appear sharper and more pronounced at $\alpha = 5^\circ$ on both the platinum and tantalum surfaces deposited. The SEM images additionally revealed interesting differences in the morphology of the platinum and tantalum structures deposited at $\alpha = 5^\circ$. Here the side-walls of the platinum structures appeared more eroded compared to the tantalum structures. This observation fitted nicely with the estimated growth exponents on the respective surfaces, wherefrom it could be concluded that surface re-emission during GLAD was more important during the thin film growth processes. The results reported here are of interests from both a fundamental perspective, since important knowledge has been gained about the mechanisms governing the growth of GLAD films. The surfaces presented here could also potentially be employed in several applied applications, where it is necessary to produce materials with a well-defined surface roughness and morphology.

Acknowledgements

We gratefully acknowledge the financial support from the Danish Research councils to the Centre for NeuroEngineering (CNE) and Interdiscplinary Nanoscience Cente (iNANO). The authors would also like to thanks Folmer Lyckegaard for the production of the thin films used in this work and the Danish Council for Independent Research (Technology and Production Sciences, 10-100118).

Reference

1. Dolatshahi-Pirouz, A. *et al.; Acs Nano*, **2010**, *4*, 2874. **DOI:** 10.1021/Nn9017872.
2. Dolatshahi-Pirouz, A. *et al.; Adv. Eng. Mater.* **2010**, *12*, 899. **DOI:** 10.1002/adem.201000120.
3. Dolatshahi-Pirouz, A. *et al.; Nanotechnology*, **2009**, *20*, 095101. **DOI:** 10.1088/0957-4484/20/9/095101.
4. Pennisi, C. P. *et al.; Nanotechnology*, **2009**, *20*, 385103. **DOI:** 10.1088/0957-4484/20/38/385103.
5. Dalby, M.J. *et al.; Nat Mater*, **2007**, *6*, 997. **DOI:** 10.1038/Nmat2013.
6. Dalby, M.J.; Riehle, M.O.; Johnstone, H.; Affrossman, S.; Curtis, A. S.G.; *Biomaterials*, **2002**, *23*, 2945. **DOI:** Pii S0142-9612(01)00424-0.
7. Dalby, M.J.; Riehle, M.O.; Sutherland, D.S.; Agheli, H.; Curtis, A.S. G.; *Biomaterials* , **2004**, *25*, 5415. **DOI:** 10.1016/j.biomaterials.2003.12.049.
8. Dolatshahi-Pirouz A.; Nikkhah M.; Kolind K.; R. Dokmeci M.; Khademhosseini A.; *J. Funct. Biomat.* **2011**, *2*, 88. **DOI:** 10.3390/jfb2030088.
9. Richert, L. *et al.; Adv Mater*, **2008**, *20*, 1488. **DOI:** 10.1002/adma.200701428.
10. Kolind, K. *et al.; Biomaterials* **2010**, *31*, 9182. **DOI:** 10.1016/J.Biomaterials.2010.08.048.
11. Pennisi, C.P. *et al.; Colloid. Surface B* , **2011**, *85*, 189. **DOI:** 10.1016/J.Colsurfb.2011.02.028.
12. Kolmakov, A.; Moskovits, M.; *Annu. Rev. Mater. Res.* **2004**, *34*, 151. **DOI:** 10.1146/annurev.matsci.34.040203.112141.
13. Aizpurua, J. *et al. Phys. Rev. Lett.* **2003**, *90*, 057401. **DOI:** 10.1103/Physrevlett.90.057401.
14. Kennedy, S. R.; Brett, M.J.; Toader, O.; John, S.; *Nano Lett*. **2002**, *2*, 59. **DOI:** 10.1021/Nl015635q.
15. GU, M.; Li, X.; Cao, Y.; *Light: Science & Applications*, **2014**, *3*, e117. **DOI:** 10.1038/Isa.2014.58.
16. Jensen, T. *et al.; Colloid Surface B*, **2010**, *75*, 186. **DOI:** 10.1016/J.Colsurfb.2009.08.029.
17. Dolatshahi-Pirouz, A.; Foss, M.; Besenbacher, F.; *J. Phys. Chem. C* **2011**, *115*, 13617. **DOI:** 10.1021/Jp202815h.
18. Dolatshahi-Pirouz, A.; *et al. Colloid Surface B*, **2008**, *66*, 53. **DOI:** 10.1016/J.Colsurfb.2008.05.010.
19. Family, F.; Vicsek, T.; *J. Phys a-Math Gen*, **1985**, *18*, L75. **DOI:** 10.1088/0305-4470/18/2005.
20. Family, F.; Vicsek, T.; Taggett, B.; *J. Phys a-Math Gen*, **1986**, *19*, L727. **DOI:** 10.1088/0305-4470/19/12/006.

21. Barabási, A.-L.; Stanley, H.E. *Fractal concepts in surface growth*. (Press Syndicate of the University of Cambridge, **1995**).
22. Zhao, Y.P.; Drotar, J.T.; Wang, G.C.; Lu, T.M.; *Phys. Rev. Lett.* **2001**, *8713*, 136102
DOI: 10.1103/Physrevlett.87.136102.
23. Pelliccione, M.; Karabacak, T.; Gaire, C.; Wang, G.C.; Lu, T M.; *Phys. Rev. B*, **2006**, *74*, 125420.
DOI: 10.1103/Physrevb.74.125420.
24. Dolatshahi-Pirouz, A. *et al.; Phys. Rev. B*, **2008**, *77*, 115427.
DOI: 10.1103/Physrevb.77.115427.
25. Dolatshahi-Pirouz, A.; Sutherland, D.S.; Foss, M.; Besenbacher, F.; *Appl. Surf. Sci*, **2011**, *257*, 2226.
DOI: 10.1016/J.Apsusc.2010.09.079.
26. Grovenor, C.R.M.; Hentzell, H.T.G.; Smith, D.A.; *Acta Metall. Mater*. **1984**, *32*, 773.
DOI: 10.1016/0001-6160(84)90150-0.
27. Hibbs, M. K.; Johansson, B.O.; Sundgren, J.E.; Helmersson, U.; *Thin Solid Films*, **1984**, *122*, 115.
DOI: 10.1016/0040-6090(84)90003-8.
28. Family, F.; *J. Phys a-Math Gen*, **1986**, *19*, L441.
DOI: 10.1088/0305-4470/19/8/006.
29. Peverini, L.; Ziegler, E.; Kozhevnikov, I.; *Thin Solid Films*, **2007**, *515*, 5541..
DOI:10.1016/j.tsf.2006.12.035.
30. Frederick, J.R.; Gall, D.; *J. Appl. Phys.* **2005**, *98*, 054906.
DOI: 10.1063/1.2035307.
31. Frederick, J.R.; D'Arcy-Gall, J.; Gall, D.; *Thin Solid Films*, **2006**, *494*, 330.
DOI: 10.1016/j.tsf.2005.08.244.
32. Robbie, K.; Sit, J.C.; Brett, M.J. *J. Vac. Sci. Technol. B*, **1998**, *16*, 1115..
DOI: 10.1116/1.590019.
33. Kennedy, S.R.; Brett, M.J.; *J. Vac. Sci. Technol. B*, **2004**, *22*, 1184.
DOI: 10.1116/1.1752903.
34. Sauerbrey, G.; *Z Phys*, **1959**, *155*, 206.
DOI: 10.1007/BF01337937.
35. Dolatshahi-Pirouz, A.; *et al. Langmuir*, **2009**, *25*, 2971.
DOI: 10.1021/la803142u.
36. Mukherjee, S.; Gall, D.; *Appl. Phys. Lett.* **2009**, *95*, 173106.
DOI: 10.1063/1.3257377.
37. Mukherjee, S.; Gall, D.; *J Appl Phys*, **2010**, *107*, 084301.
DOI: 10.1063/1.3385389.